WILEY | Hindawi

Research Article

Effect of the Number and Distribution of Circular Holes on the Damage and Fracture of Limestone Using PFC2D

Handong Liu,[1] **Shuai Liu** [iD],[1,2] **Haining Liu,**[1] **Yunyou Fu,**[3] **Minglei Kang,**[3] **Zhe Bai** [iD],[4] **Jianglong Xu,**[5] **and Chao Zheng**[4]

[1]*Henan Key Laboratory of Geomechanics and Structural Engineering, North China University of Water Resources and Electric Power, Zhengzhou 450046, China*
[2]*College of Geosciences and Engineering, North China University of Water Resources and Electric Power, Zhengzhou 450046, China*
[3]*North Henan Water Conservancy Project Management Bureau, Xinxiang 453005, China*
[4]*School of Civil and Transportation Engineering, Henan University of Urban Construction, Pingdingshan 467036, China*
[5]*Hetaoyu Branch of Fushun Mining Group, Qingyang 745399, China*

Correspondence should be addressed to Shuai Liu; austin-shuai-liu@qq.com

The common occurrence of various number and distribution of hole flaws complicates the mechanical behavior and fracture mode of the rock masses that contain them. This study develops seven numerical models of limestone samples with different numbers and distributions of circular hole flaws using 2-D particle flow discrete element code (PFC2D) to investigate their impact on the mechanical properties of limestone while maintaining the same flaws area. In addition, it analyzes the effect of these factors on the mesomechanical features of each model, including the characteristic stress values (peak stress, crack initiation, and damage stress), crack evolution, stress, and displacement field. The results showed that the peak stress, crack initiation, and damage stress of the single-hole model are between those of multihole models. As the arrangement of dip angle increases, the peak stress, crack initiation, and damage stress of models with the same number of multihole flaws exhibit a V-shaped change. The characteristic stress values are the largest when the holes are vertically aligned. Model differences in crack development path, shape, and number, as well as stress concentration area and failure mode, are primarily due to the number and distribution of holes. The circular holes are arranged at approximately 45°, and the greater the number of defects, the more likely the model is to fail. The study's findings can provide support and reference for the research system of deformation and failure of rock mass with hole flaws.

1. Introduction

Under different geological processes, naturally occurring rock masses often contain various holes, fissures, and other flaws [1, 2]. For example, in limestone areas, small karst caves with diverse distribution patterns are common [3, 4]. These flaws are often numerous and randomly distributed, making the physical properties, deformation, and failure behavior of the rock mass that contain them complex and dynamic. This seriously affects the stability and security of rock masses during construction [5–7]. Consequently, it is necessary to investigate the effect of the number and distri-

bution of hole flaws in limestones on their damage-deformation-failure behavior.

Researchers have obtained many positive results in studying rock masses containing holes. The variable factors related to hole flaws are hole shape [8], hole size [9], hole number [10, 11], and their combination with other flaw types [12, 13]. Zeng et al. [14], Gui et al. [15], and Xia et al. [16] applied the discrete element numerical simulation method to analyze the influence of a single-hole flaw with multiple regular forms (circular, square, and trapezoidal) on the mesomechanical properties and failure mode of a rock mass. Li et al. [17] utilized digital image correlation to

record and discuss the deformation and fracture of marble containing circular and elliptical holes. Zhao et al. [18] proposed a failure strength model for brittle materials with single circular hole flaws by improving the Sammis-Ashby model [19] and using a numerical model to test and verify the modified model. Similarly, Lin et al. [20] analyzed the failure mode of multiple-holed granite subjected to uniaxial loading and developed the Sammis-Ashby model. Yang et al. [21] and Tian et al. [22] examined the different distribution patterns of two elliptical holes based on laboratory and PFC2D simulation tests; they investigated the effect of hole spacing and hole arrangement angle on the damage evolution and failure mechanism of sandstone. Du et al. [23], Zhao et al. [24], and Ma et al. [25] conducted uniaxial compressive strength (UCS) tests on rock samples with two holes and studied the strength and crack propagation features of samples under various hole spacing configurations and different dip angles.

For comparative analysis of the different number of hole flaws, it is common for most researchers to list one to three holes. For example, He et al. [26] compared red sandstone's energy evolution and mechanical behavior with one to three circular holes under loading and unloading states. Tang et al. [27] conducted experiments on rock material with single and three-round holes and simulated the splitting failure observed in the test samples. Liu et al. [28] used PFC2D to reveal the damage evolution and distinguishing strength features of a composite rock mass when the weak interlayer contained one to three square holes and conducted research on the filling and reinforcement of the holes. Wong et al. and Wong and Lin [29, 30] conducted an array of indoor tests on rock samples with one, three, and multiple circular holes and investigated the failure mode and distinguishing strength features of rock samples with various distributions of circular holes. Gui et al. [31] developed single circular and multicircular hole numerical models with staggered distributions of various circular hole aperture sizes and numbers. They systematically analyzed the effect of the number and distribution of hole flaws on the mechanical behavior of the rock containing them. Huang et al. [32] drilled three noncollinear holes in granite samples and analyzed the rock samples' crack development and failure regularity with a specific arrangement and combination of multiple small circular holes. Jespersen et al. [33] conducted laboratory tests and numerical simulations on gypsum specimens with seven uniformly distributed circular holes and discussed the effect of large hole spacing and arrangement on the strength and failure mode of the samples. Lin et al. [20] and Huang et al. [34] performed UCS tests on granite rock samples, including multiple holes, and focused on the impact of the holes on crack initiation, propagation, and coalescence. Using AE technology combined with PFC2D numerical simulation, the failure mechanism of the rock samples was revealed.

The studies above have achieved fruitful results regarding the mechanical properties of lithosome containing hole flaws and introduced scientific and reliable research approaches such as the PFC2D method. Existing research on the quantity and distribution of hole flaws focuses primarily on holes of the same size. For example, in previous studies, the size of the single versus multiple-hole flaws in the rock sample was the same, or the influence of a fixed number of holes on the rock's strength properties was investigated. However, increasing the number of holes will inevitably raise the total defect area in the rock mass, and rock samples will undoubtedly deteriorate. With the increase in the number of holes, the overall distribution of holes in the rock mass will inevitably change, and the distribution and number of holes are organic and unified research factors. The above literature indicates that few studies have been conducted on the influence of the number and distribution of holes on the fracture and distinguishing failure features of rock samples with the same flaw area. In addition, there is little research on the distinguishing mesomechanical features of rock, such as damage stress, based on the distribution and number of holes. Under the same total area of hole flaws, the design and analysis of different numbers and distributions of holes can more accurately represent the scientific nature of the research on their influence on the mechanical properties of a rock mass. Under the assumption of equal hole flaw area, this paper numerically simulates the mesomechanical properties of limestone samples with various numbers and distributions of circular holes using PFC2D code to reveal the damage and deformation mechanism of a rock mass.

2. Mesoparameter Calibration and Numerical Models

2.1. Determining of the Macro-Mesoparameters of Limestone. The parallel bond model in the PFC2D code was applied to simulate the rock material numerically, because it can simultaneously transfer force and moment and has an extensive contact range [35–37]. Using the parallel bond model will result in issues such as low compressive-tensile strength ratio and internal friction angle. However, modifying the parallel bond failure criteria to reduce the moment contribution of bond stress has solved the above problems better. The particle flow discrete element numerical simulation method has become exceedingly reliable and scientific in international rock mechanics [38, 39]. In order to determine limestone's macro and mesoscopic parameters, its macroscopic physical and mechanical parameters must first be determined through laboratory tests. The laboratory tests in this study were conducted according to the ISRM specification [40]. In the UCS test, cylindrical rock samples with standard dimensions of 50 mm in diameter and 100 mm in height were used, and the axial deformation rate was set for loading to 0.001 mm/s. After obtaining the limestone's basic physical and mechanical parameters, an isologous model was developed for the numerical simulation test and comparison. The mesoscopic parameters in the PFC2D code were repeatedly adjusted until the results of the experimental and numerical tests were perfectly consistent [41, 42]. Figure 1 depicts the limestone rock sample and its typical uniaxial compression numerical model and parallel bond contact in the PFC2D code.

The UCS test was performed on the established numerical model of the intact rock sample using the identical
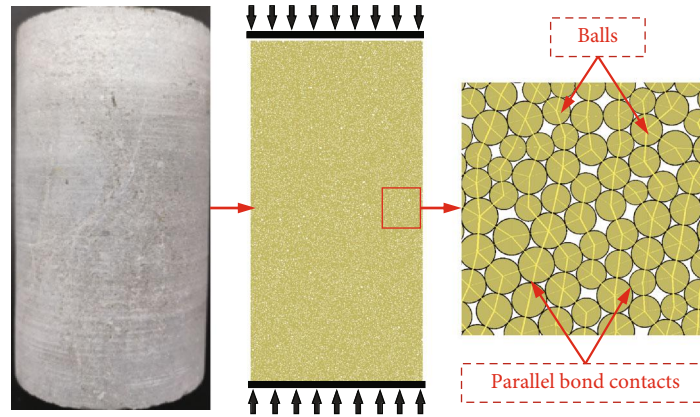
Figure 1: Limestone rock sample and corresponding intact numerical model.

method and loading conditions as the physical experiment. Figure 2 illustrates the results of comparing the failure forms and uniaxial stress-strain curves of the rock models in the experimental and numerical tests. The peak strength and deformation modulus of the stress-strain curves of the experimental and numerical samples are identical, and the failure modes of the two are similar. This demonstrates that the microscopic parameters in the PFC model can accurately simulate the mechanical properties of macro rock samples [43]. The microscopic parameters are obtained as shown in Table 1.

2.2. Establish Numerical Models. The area of the holes in the established models remained unchanged, while the holes' number and location were altered to illustrate better the effect of the number and distribution of holes on the mechanical features of the rock samples. Circular holes are a representative flaw shape in rock masses, so the hole shape in the models in this study was set as circular. The aperture diameter for a single circular hole is 15 mm (the hole area is about 1.77 cm^2), so the aperture diameters for two and three circular holes are approximately 10.61 mm and 8.66 mm, respectively. In the models, the arrangement and distribution of two and three circular holes in the horizontal, 45°, and vertical directions are considered, along with the setting of equal distances between the hole boundaries and the circular holes and the model boundary. Thus, seven numerical models, designated NM-1 through NM-7, were established for the rock samples with circular hole flaws. Figure 3 depicts the numerical models. The NM-1 model contains a single-hole flaw with a diameter of 15 mm in the model's center. NM-2 includes two circular holes with a horizontal distribution, and the distance between the two holes and the left and right boundaries of the model is equal (about 9.60 mm). NM-3 contains two circular holes arranged at 45° in the middle, and the distances between the two circular holes and the left and right boundaries of the model are about 16.50 mm. Two circular holes are arranged vertically in the center of the NM-4 model, and the distances between the two circular holes and the upper and lower boundaries of the model are about 26.26 mm. Similar to NM-2 to NM-4, NM-5 to NM-7 contains three circular holes with a diameter

of 8.66 mm, and the distances in the horizontal, 45°, and vertical directions were 6.01, 11.18, and 18.51 mm, respectively.

2.3. Method for Monitoring the Cracks and Simulating the Acoustic Emission. The cohesion of particles is determined in the PFC2D code by the normal bond strength (n_bond), tangential bond strength (s_bond), and friction coefficient between particles [44–46]. When the transmitted stress exceeds the bond strength between rock particles, the contact bond between particles is destroyed under the load, and microcracks appear in the numerical model [47–49]. As the microcracks continue to expand in the model, the deformation energy will be released, forming acoustic waves. In this study, the AE events were simulated based on the change in the number of cracks generated in the PFC2D code, i.e., the AE hits were generated during the breaking of the contact bonds [50, 51].

During the damage evolution of rock samples, crack initiation and damage stress are significant boundary values representing the rock's strength. This study utilized the method of monitoring crack development and evolution to represent the damage stress and crack initiation stress, and the two define the boundary points of different periods in the crack growth process. The crack initiation stress refers to the original cracks in the compacted rock, after which the latent cracks begin to sprout and grow. Meanwhile, a crack was just initiated in the model, and the stress value corresponding to the first crack's initiation was monitored [28, 52]. The damage stress refers to the convergence and connection of the initial and expanded microcracks in the previous stage, resulting in an unstable propagation of cracks. From this time until the peak stress in the model, the number of cracks shows a continuously increasing acceleration trend, and the corresponding AE events also begin to have a continuous and greater stable activity [53]. Previous studies [54–56] have revealed that the damage stress and crack initiation stress determined by the method of monitoring microcracks are identical to the results of laboratory tests. Although the simulated AE events cannot achieve the mechanical response state of a real rock mass, the reflected change aids in understanding the AE phenomenon of the rock.
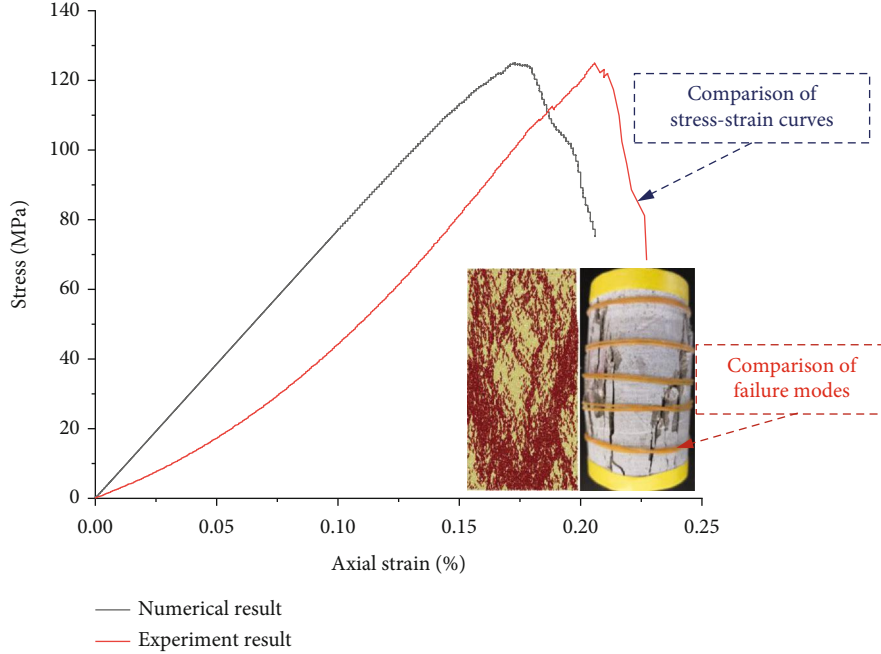
FIGURE 2: Verification of the experimental and numerical results.

TABLE 1: Microscopic parameters of the rock.

Parameters	Rock (value)
Minimum particle diameter (mm)	0.2
Particle diameter ratio	1.5
Grain density (g/cm^3)	3.05
Contact modulus of the particle (GPa)	36.21
Contact bond gap (mm)	0.05
Porosity	0.1
Parallel bond friction angle (°)	42.5
Parallel bond tensile strength (MPa)	10.95
Normal critical damping ratio	0.5
Parallel bond cohesive force (MPa)	52.23

3. Analysis of Simulation Test Results

3.1. Analysis of AE Events and Characteristic Stress Values of each Model. The stress-strain, AE, and the totality of cracks for each model are summarized together, and the three characteristic stress values of crack initiation stress, damage stress, and peak stress of each model are marked on the stress-strain curve. The stress-strain-acoustic emission-crack number curves of each model are obtained, as shown in Figure 4. The crack initiation, damage, and peak stress are denoted by σ_{ci}, σ_{cd}, and σ_c, respectively. Table 2 lists the values of the crack initiation, damage, and peak strain-stress of the models.

The curves in Figure 4 reveal that the UCS of the intact model is about 125.05 MPa, while the uniaxial compressive strengths of NM-1 to NM-7 are about 84.68, 70.15, 70.51, 92.28, 69.52, 63.86, and 94.35 MPa, respectively. The strength of the intact model is the largest, and the UCS of

NM-1 to NM-7 is significantly reduced. Given the numbers and distribution of hole flaws, the UCS of the models containing the circular hole flaws is different, and the UCS of the two models with the vertical arrangement of circular holes is high. The strength of NM-2 and NM-3 is equivalent, while the strength of NM-5 is greater than that of NM-6. This indicates that when the two circular holes are arranged at 45°, the influence of the related flaw types, such as fissures and soft structural planes, on the rock mass is different [57, 58]. The main reason for this is that although the two circular holes are arranged at a 45° dip angle, the spacing between the circular holes is still relatively large, and penetration under uniaxial compression is insufficient. When the three circular holes are arranged at 45°, the distance between them decreases, and the effect of promoting the failure of the rock samples increases, resulting in a reduction in its bearing capacity; therefore, the NM-6 model has the smallest UCS of all the models. In general, the strength of the two-hole model with the horizontal and 45° distribution of holes is stronger than that of the corresponding three-hole model. However, when the circular hole flaws are arranged in the vertical direction, the UCS of the model with the three vertical holes is the largest, and the intact model is reduced by 24.55%. The strength of the model with the two holes is the second smallest, and the UCS of the intact model decreases by 26.21%. The three-hole model with the 45° inclination angle has the smallest UCS, which is 48.93% lower than the intact model.

In the AE characteristic histograms of each model, the AE events do not occur when the initial loading stress is minor. As the loading stress increases, cracks appear within the rock sample, and acoustic emission phenomena appear in each model. The crack initiation stress of each model is about 48.16, 13.50, 14.99, 10.54, 15.67, 17.23, 11.35, and
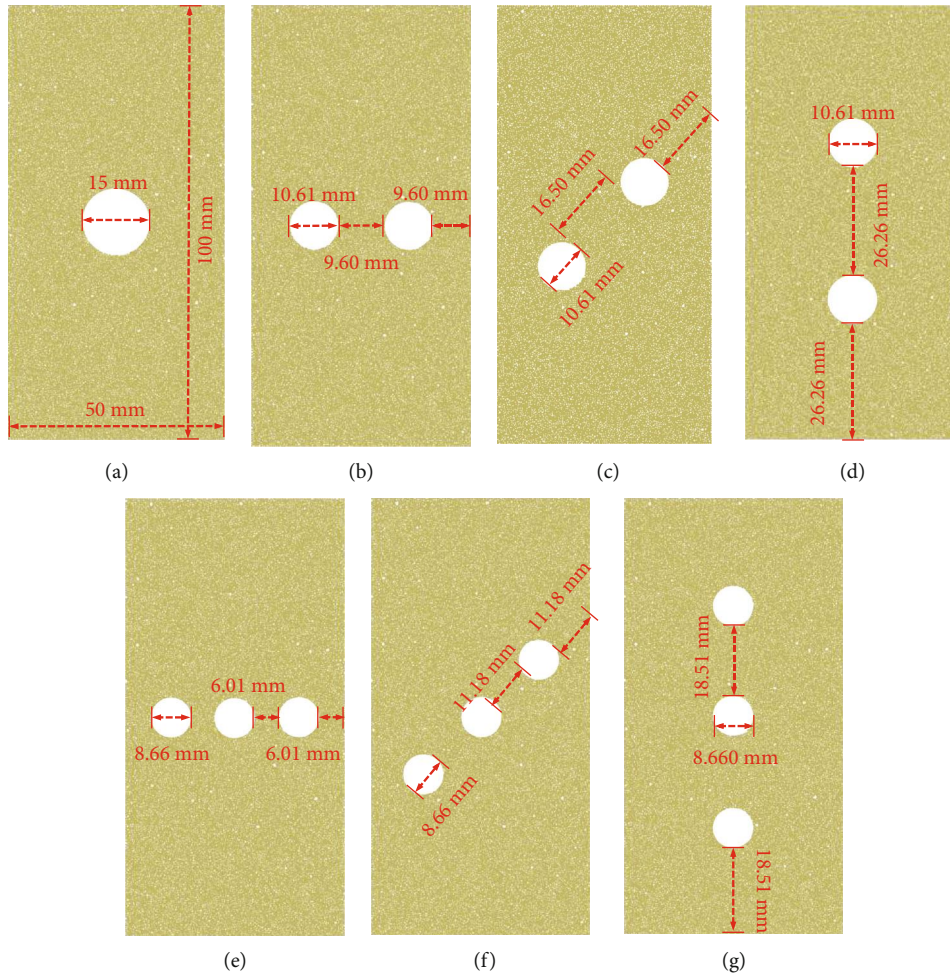
FIGURE 3: Numerical simulation models: (a–g) represent the numerical models NM-1 to NM-7, respectively.

20.27 MPa, respectively. The hole flaws significantly reduce the crack initiation stress of the models and cause the AE events to occur earlier. Two-hole and three-hole models with the 45° arrangement begin to exhibit AE activity at strains of 0.0156% and 0.0170%. Internal cracks in the rock samples gradually develop and expand with continuous loading, and the number of cracks maintains a stable growth rate. The number of AE counts of each model also continues to increase slowly. When loading to 70%-80% of the peak stress, the totality of cracks in each model gradually begins to increase rapidly, and the number of AE also counts suddenly increases. At this time, the model is considered to have reached the damage state, and the corresponding stress level is the damage stress. The damage stress of each model is about 106.52, 61.43, 55.59, 52.87, 68.44, 52.75, 49.96, and 73.30 MPa, respectively. The damage stress of the models with circular hole flaws is significantly reduced compared to the intact model, while the damage strain is also significantly increased. In terms of the damage changes and the crack initiation stress, the variations under various distributions of the two and three circular holes are similar, with the smallest changes occurring when the holes are arranged at 45°. Accordingly, the damage degree is greater under the same loading condition, and the values are the largest when

the holes are distributed vertically, resulting in a lower damage degree. After the damage stress of each model is reached, the total number of cracks in each model increases rapidly, and the number of acoustic counts rises sharply at the peak stress, where it reaches the maximum. The acoustic emission is "active" around the peak stress until the postpeak failure stage, and the AE events are concentrated around the peak stress. The number of cracks in each model increases rapidly again, but the total number of AE counts decreases in the postpeak stage. Overall, the intact model has the highest number of AE counts and the most concentrated AE event distribution. Each model's maximum number of AE counts is small, and the AE events are scattered around the peak stress. The distribution and number of the circular hole flaws also influence the distinguishing AE features. They affect the early and late occurrence of AE events at the crack initiation stress level and the number of acoustic emission shots at the peak stress. The changing trend is equivalent to each model's peak stress, and the model's AE events with the circular holes arranged vertically are active.

3.2. Analysis of Crack Evolution. Based on the description of the total number of cracks in Figure 4, to better show the crack evolution in each model, the crack growth in each
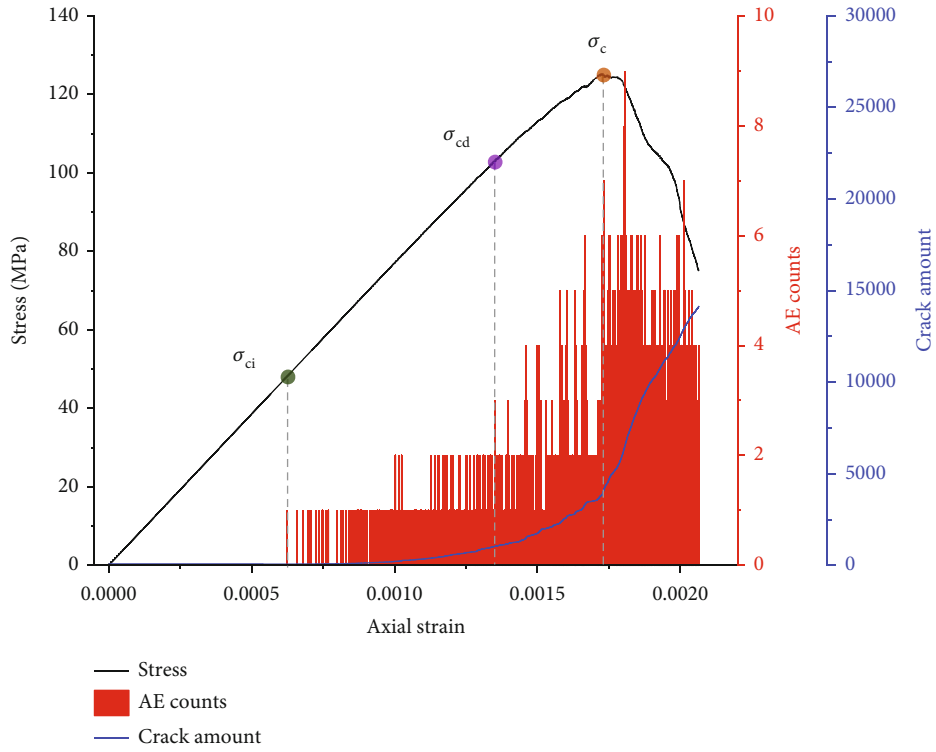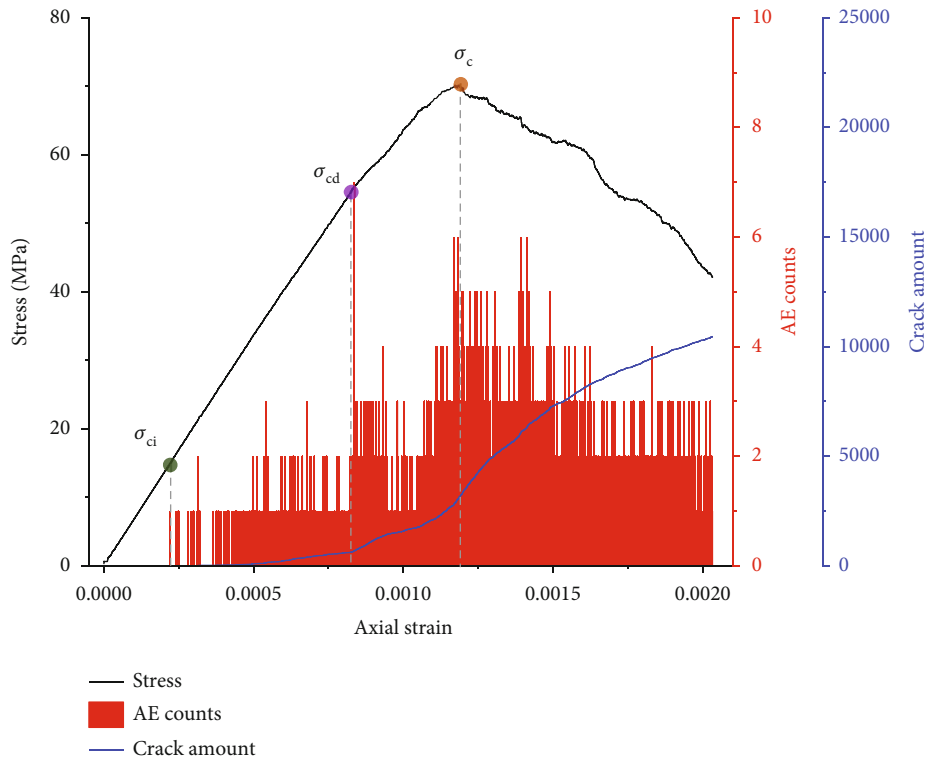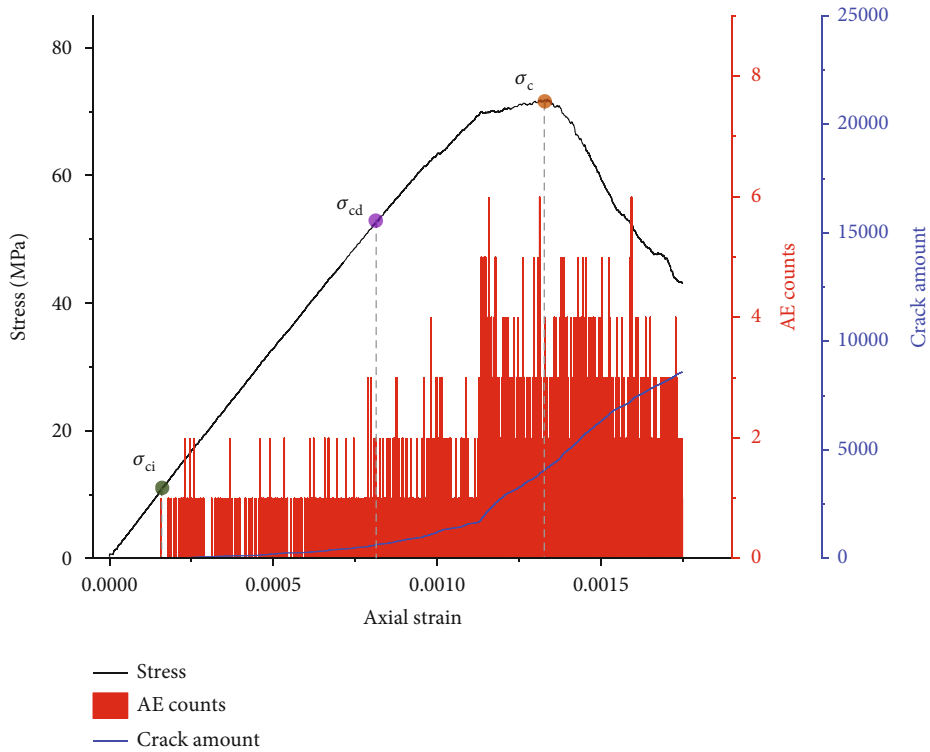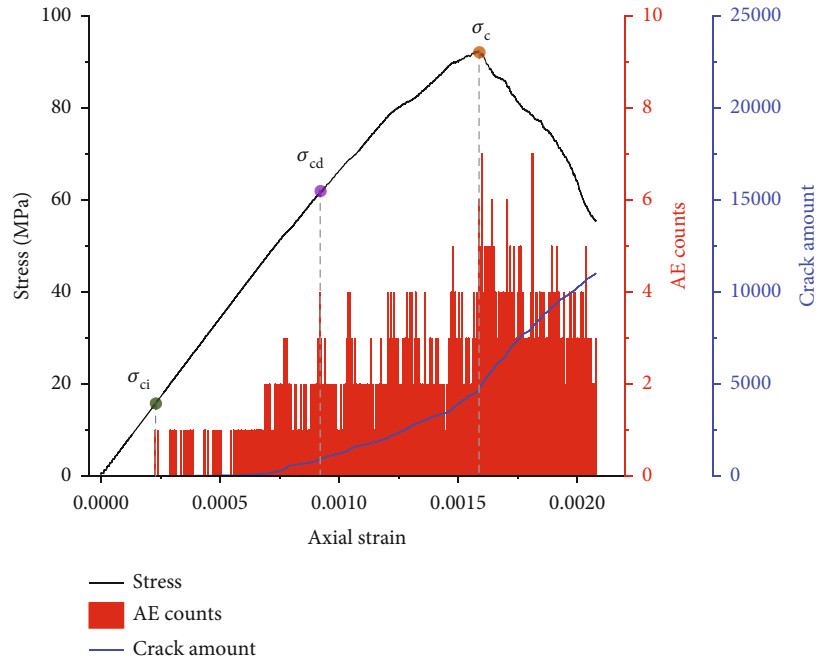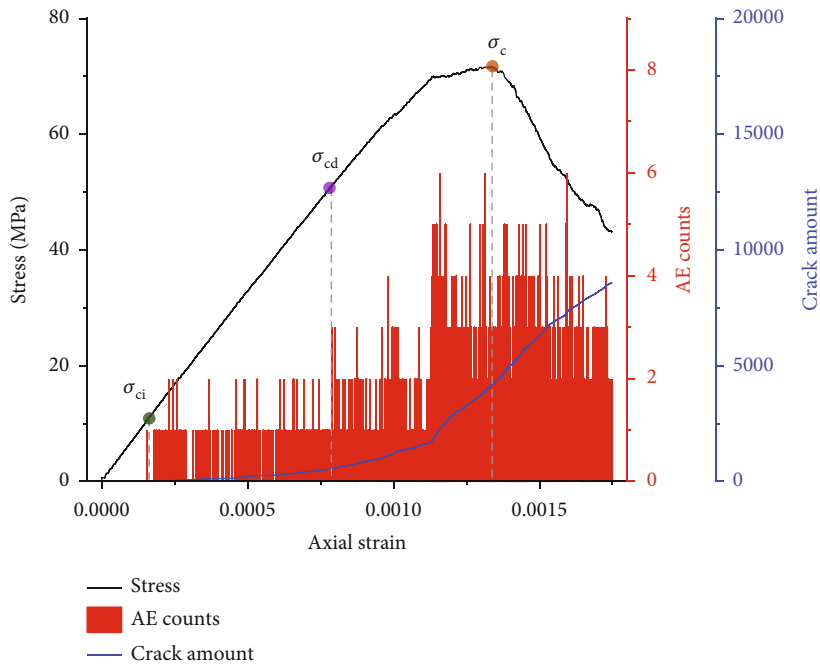
(a)
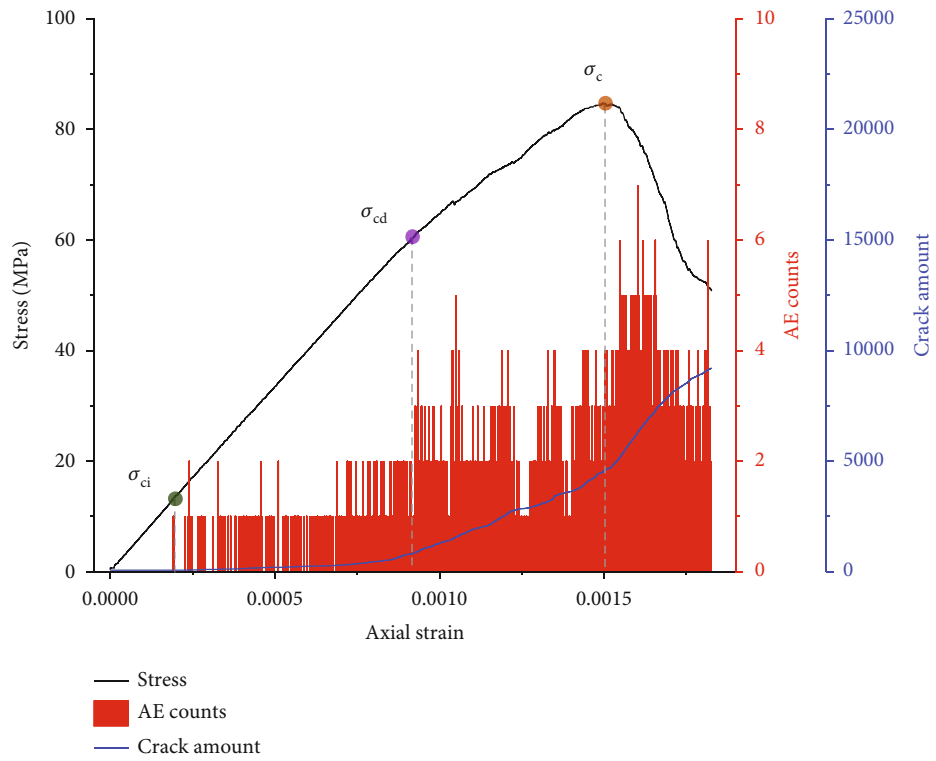
(b)

Figure 4: Continued.

(c)

(d)

Figure 4: Continued.

(e)

(f)

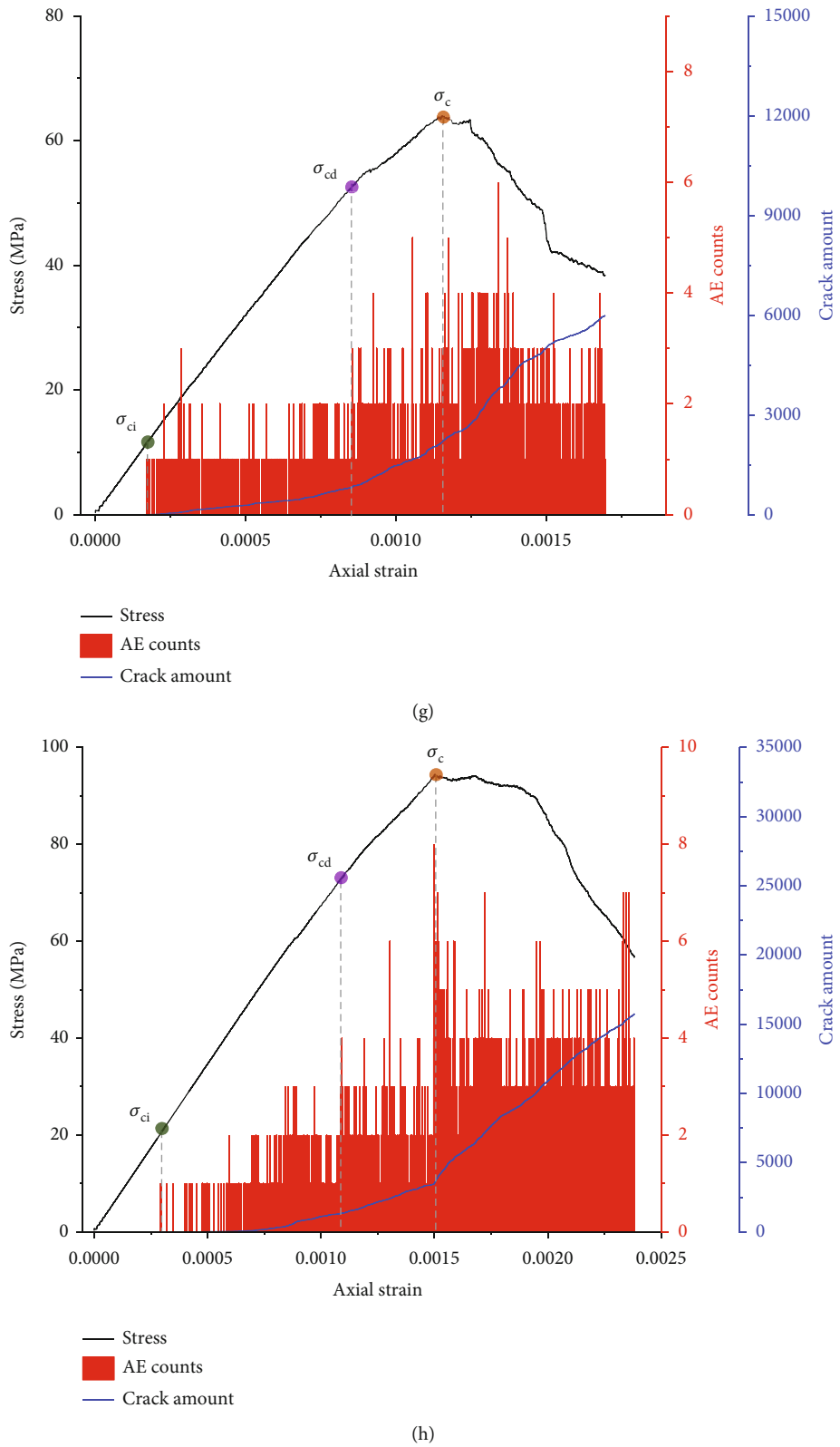Figure 4: Continued.

(g)

(h)

FIGURE 4: Stress-strain-acoustic emission-crack number curves of each model: (a) represents the intact model; (b–h) represent the NM-1 model to the NM-7 model, respectively.

model is analyzed from the perspective of the crack initiation stress, damage stress, peak stress, and 60% of the UCS stress level after model failure. The distinguishing crack evolution features of each model are shown in Figure 5. The tensile cracks are depicted in red, while the shear cracks are depicted in black.

TABLE 2: Crack initiation, damage, and peak stress and strain of each model.

Model name	Crack initiation strain (%)	Crack initiation stress (MPa)	Damage strain (%)	Damage stress (MPa)	Peak strain (%)	Peak stress (MPa)
Intact model	0.0625	48.16	0.1402	106.52	0.1727	125.05
NM-1	0.0192	13.50	0.0934	61.43	0.1498	84.68
NM-2	0.0221	14.99	0.0841	55.59	0.1185	70.15
NM-3	0.0156	10.54	0.0818	52.87	0.1376	70.51
NM-4	0.0227	15.67	0.1034	68.44	0.1583	92.28
NM-5	0.0257	17.23	0.0802	52.75	0.1131	69.52
NM-6	0.0170	11.35	0.0805	49.96	0.1152	63.86
NM-7	0.0292	20.27	0.1095	73.30	0.1501	94.35

The crack initiation in the models with hole flaws primarily occurs at the top and bottom points of the circular holes, and each model has tensile cracks. The existence of the circular hole flaws is the main factor that induces the early initiation of the cracks. When the damage stress of each model is reached, the number of cracks in the intact model increases, the crack distribution becomes more dispersed, and a small number of shear cracks appear. The cracks in the NM-1 to NM-7 models are gathered around the circular holes, and the crack distribution patterns are distinct due to the influence of the varying number and distribution of circular holes. For example, in the NM-1 model, the cracks exhibit an "Ж"-shaped distribution centered on the single circular hole, while in the NM-2 model, the cracks are mainly distributed above and below the two circular holes and concentrated in the middle part of the vertical direction of the model, resulting in greater crack propagation in the middle part. A small number of shear cracks appear in each flawed model under damage stress, and they are concentrated near or between the circular holes. At the peak stress, cracks continue to develop and propagate along the distribution state of the damage stress in all the models. In the NM-1 through NM-7 models, the cracks at the upper and lower points of the circular holes spread slowly and are near the circular holes. These cracks propagate faster through the circular holes and penetrate the entire model. However, the models are in the limit equilibrium state, and the cracks are about to penetrate and destroy the model. The number of shear cracks shows a particular increase, and the distribution range is still mainly gathered around or between the holes at the peak stress. At the postpeak failure stage, the extensive cracks in each model develop rapidly and form a concentrated area of crack penetration, affecting each model's failure path.

3.3. Variation of the Vertical Stress Field. In order to investigate the distinguishing stress field evolution features of each model, the vertical stress field is analyzed under various stress levels. 10%, 50%, 100%, and 60% of the UCS in the postpeak failure stage are selected to illustrate the distinguishing distribution features of the stress field in each model, as shown in Figure 6.

Figure 6(a) indicates that the stress concentration of the intact model before the peak stress is uniformly distributed in the entire model and only slightly dispersed until peak stress. The stress concentration area in the postpeak stage shows a roughly "conical" distribution, and the main distribution area of the low stress is located in the lower right corner of the model. Before the peak stress, in the NM-1 to NM-7 models, regardless of the size and distribution of the circular hole, there is a compressive stress concentration phenomenon on both sides of the holes. In contrast, the area above and below the circular hole is a low-stress or tensile stress area. With the increase in the loading stress, the compressive stress concentration region on the two sides of the circular hole shows a decreasing trend, but the degree of stress concentration is greater. The low-stress or tensile stress area above and below the circular hole shows a gradually expanding trend. At the peak stress, the compressive stress concentration region of the NM-1 model is distributed in the form of a "butterfly" centered on the circular hole. The maximum concentration stress is still close to the two sides of the circular hole, and the maximum concentration stress is about 191.68 MPa. The maximum compressive stress concentration area between the two horizontal circular holes in the NM-2 model is gradually fused, and the maximum concentration stress is about 187.67 MPa. The maximum stress concentration area in the NM-3 model is located between the two 45° arranged circular holes and they are connected, while the stress concentration area outside the two circular holes diffuses outward to the model. In the NM-4 model, the large stress concentration region spreads away from the positions on both sides of the circular hole, focusing primarily on both sides of the model. The low-stress area above and below the hole also extends to an area between the top and bottom of the model and two holes. At peak stress, the stress concentration distribution of the NM-5 to NM-7 models is comparable to that of the NM-2 to NM-4 models. In the postpeak failure stage, the stress concentration areas in each model with hole flaws are significantly reduced, and the low-stress areas above and below the circular hole penetrate the entire model. It is worth noting that in the NM-4 and NM-7 models, the compressive stress has a wide range of stress concentration on both sides of the model, whether at the peak stress or after the postpeak stage. This demonstrates that the models have good bearing capacity, which is also the reason why both models have high uniaxial compressive strengths.
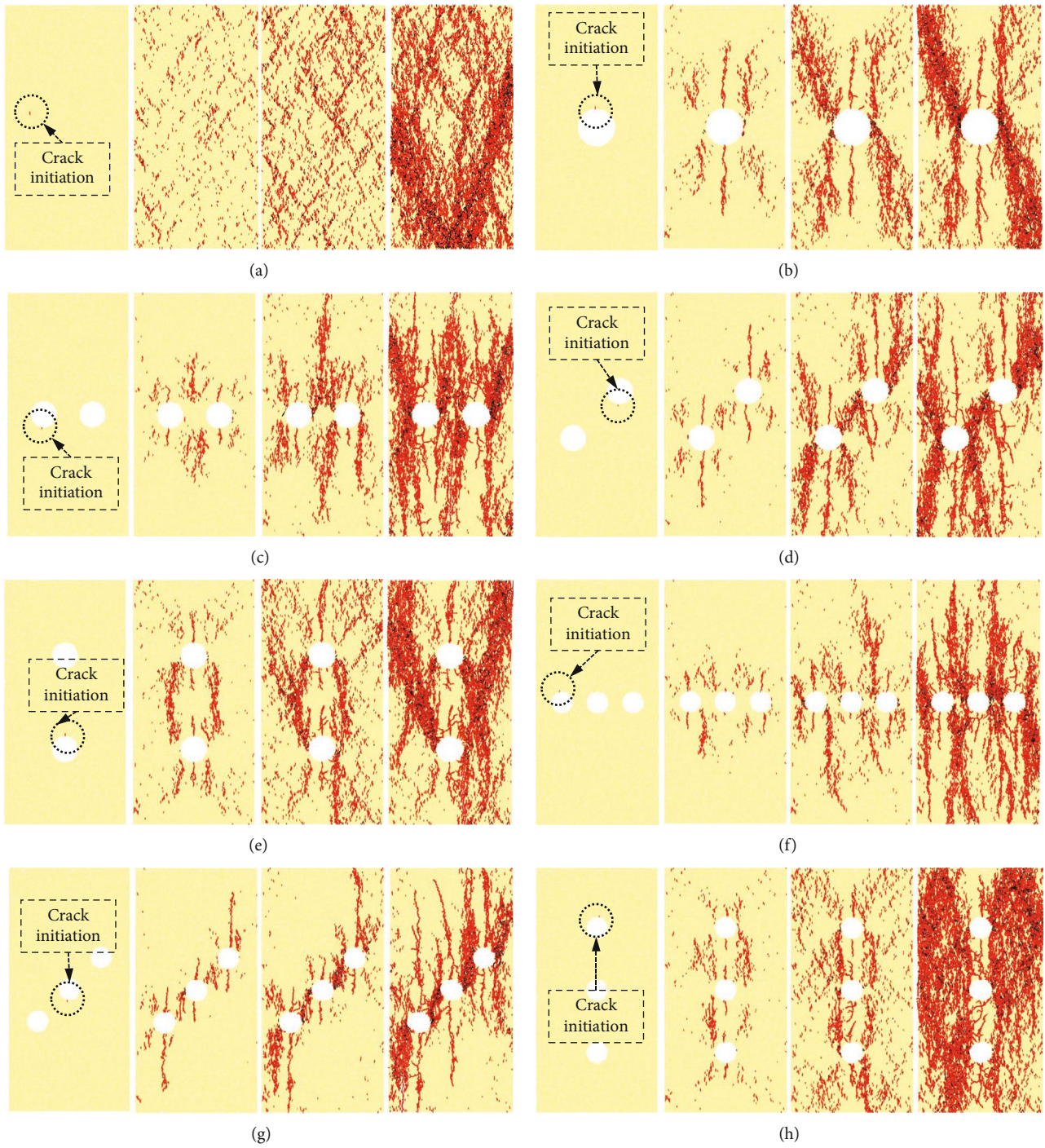
FIGURE 5: Crack evolution characteristics in each model: (a) represents the intact model; (b–h) represent the NM-1 model to the NM-7 model, respectively.

3.4. Displacement Field Evolution and Failure Mode. To analyze and compare the change of the displacement field and the distinguishing features of each model's deformation and failure process, 50% of the UCS, peak stress, and 60% of the UCS in the postpeak failure stage of each model are selected. Variations in the displacement fields of each model are shown in Figure 7.

Figure 7 indicates that under uniaxial compression, the displacement field of the intact model before failure is the smallest in the middle of the horizontal direction, and the displacement gradually increases towards the top and bottom of the model. The top and bottom are the maximum displacement area of the model. The displacement field is distributed symmetrically along the horizontal centerline of the model. During the failure period, the displacement at both ends of the bottom of the model is large, and the model's small and medium displacement areas exhibit a "V" type distribution. The overall failure mode of the model
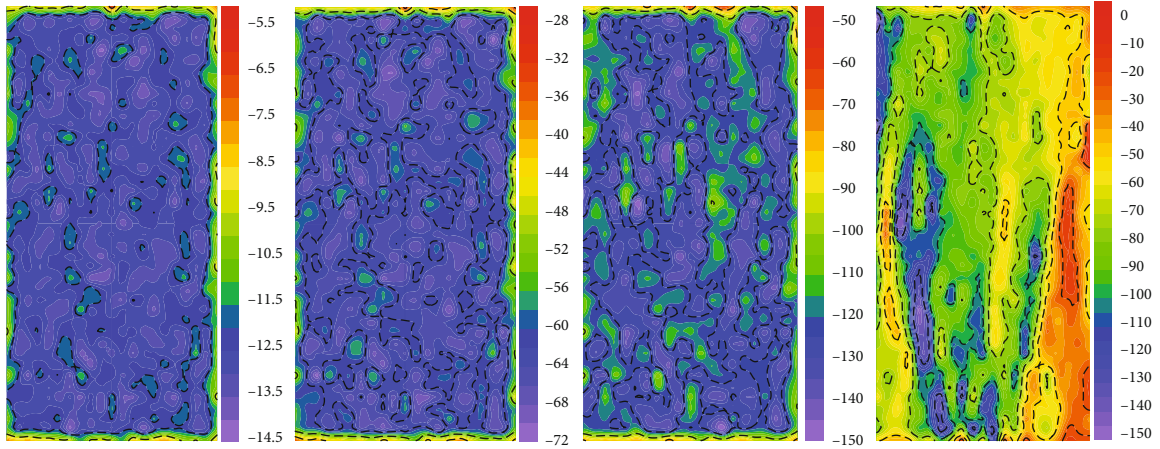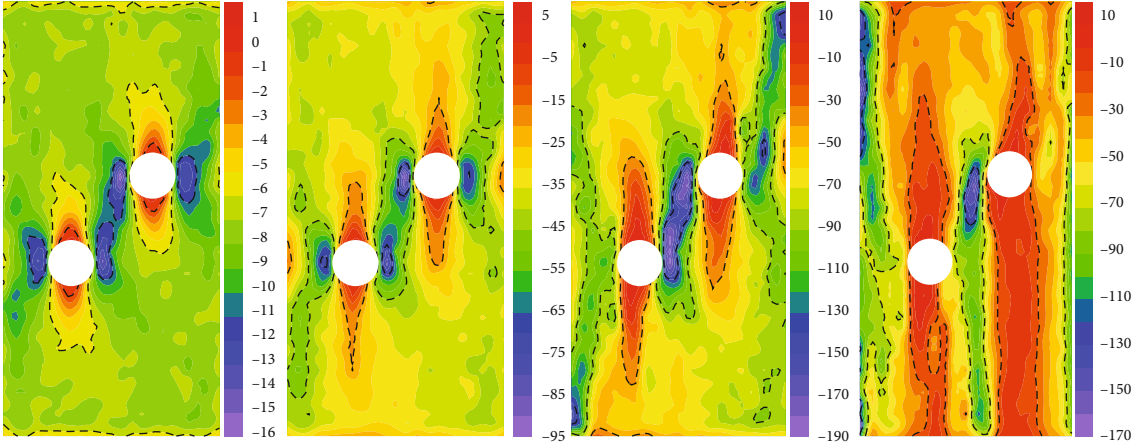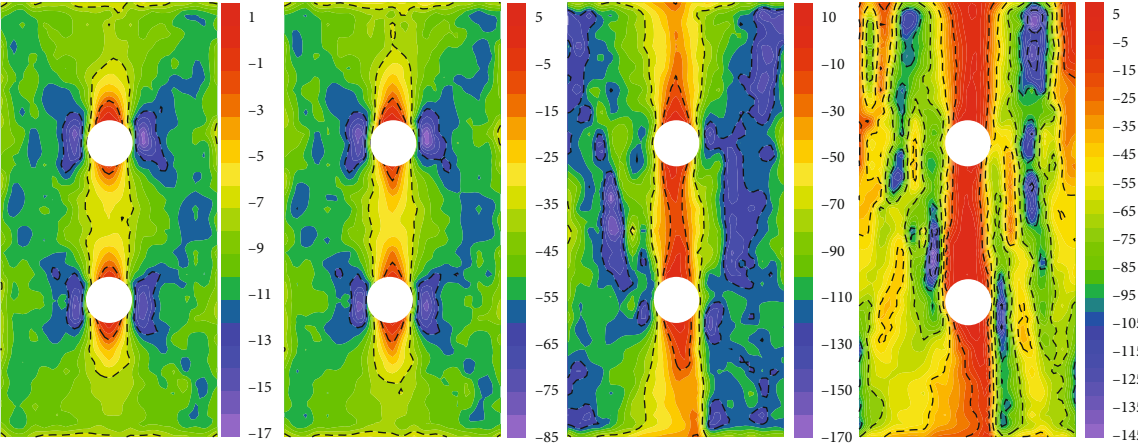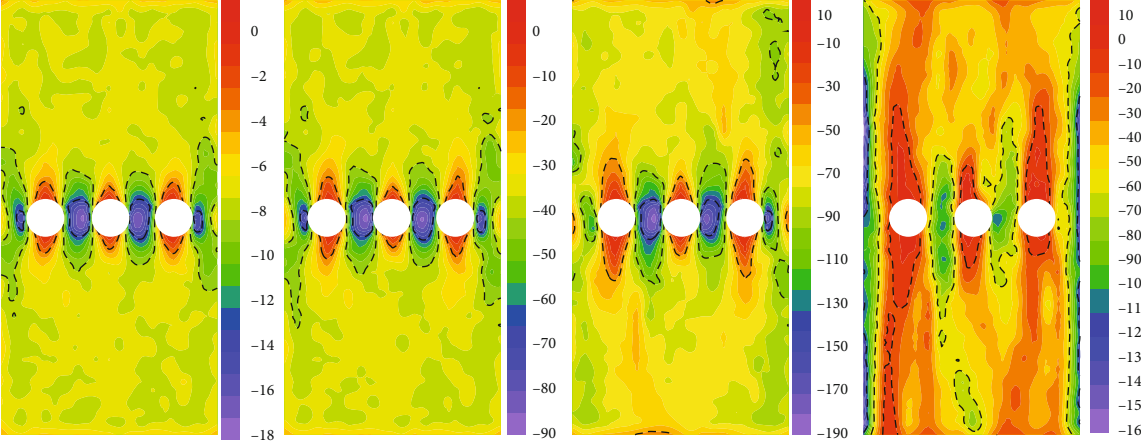
(a)
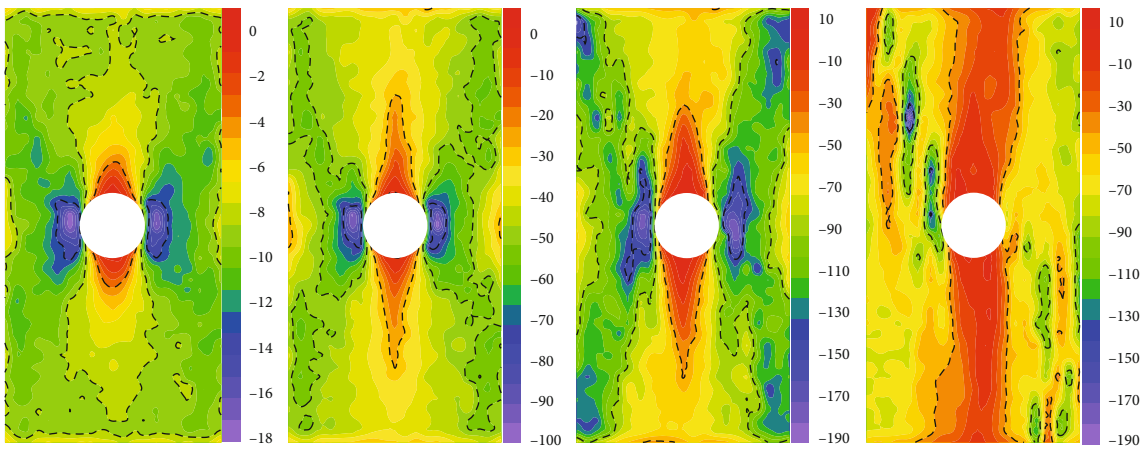
(b)
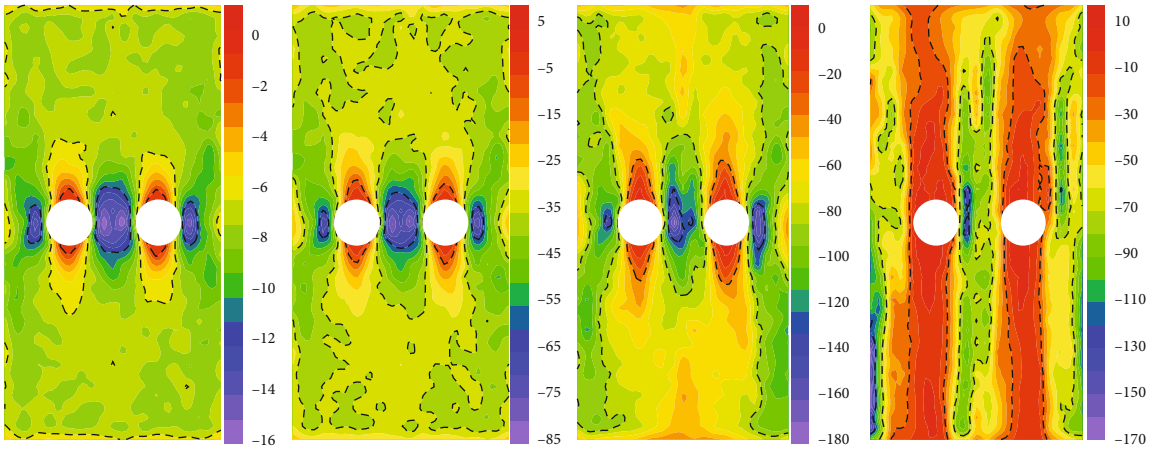
(c)

Figure 6: Continued.

(d)
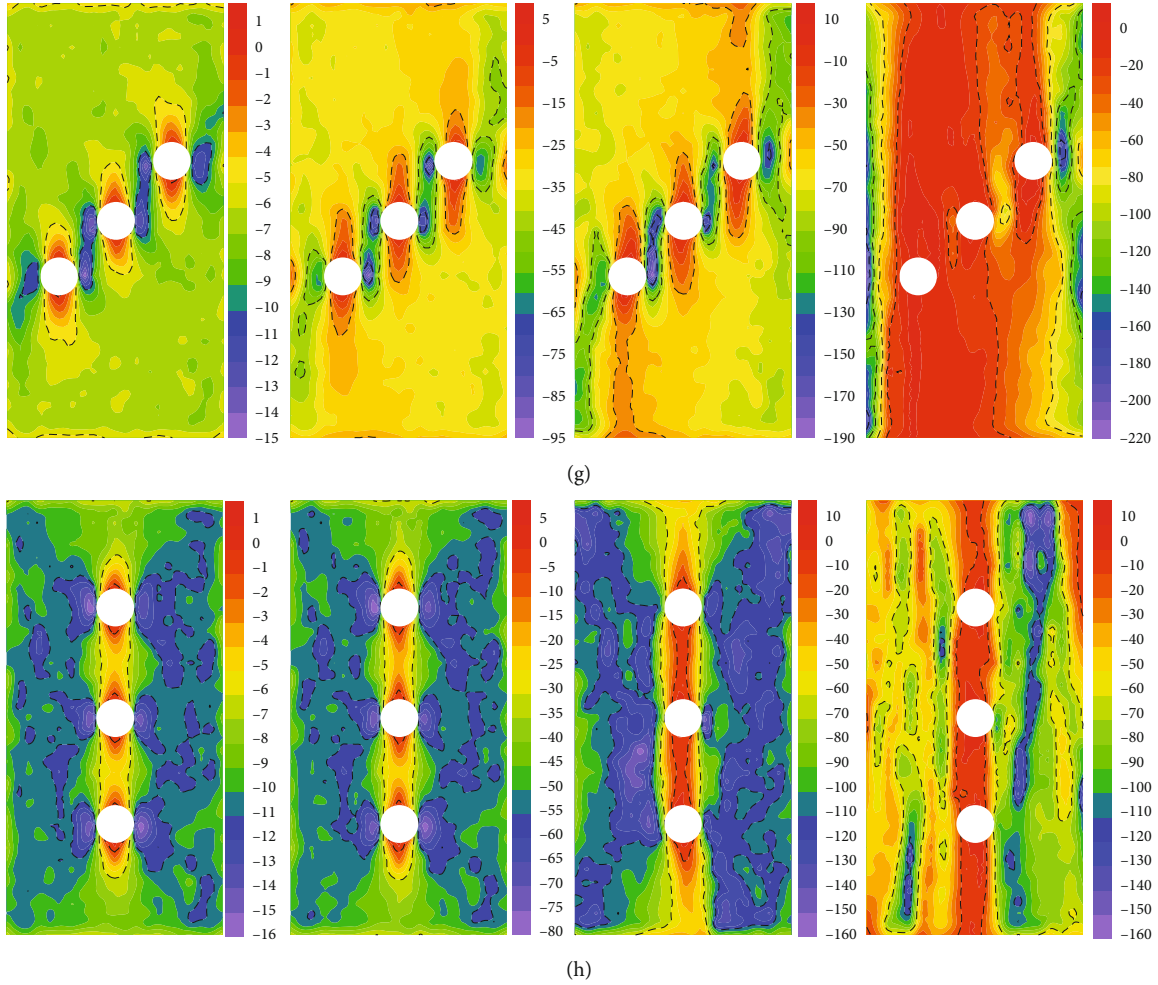

(e)

(f)

Figure 6: Continued.

(g)

(h)

FIGURE 6: Distinguishing distribution features of the vertical stress field: (a) represents the intact model; (b–h) represent the NM-1 to the NM-7 model, respectively.

is conical, which corresponds to the crack concentration area during the failure period of the intact model. When the NM-1 model is at 50% of the UCS, the displacement field is also symmetrically distributed along the model's horizontal centerline, and areas with small displacements appear on either side of the circular hole. Additionally, the small-displacement change areas on both sides are distributed symmetrically along the circular hole in an "M" shape. When the load reaches its peak stress, the displacement of the small displacement area in the model gradually increases and spreads, forming an "X"-shaped small-displacement area. At the failure stage, the model displays inclined splitting failure along the vicinity of the circular hole. In the NM-2 to NM-4 models, the maximum displacement before peak stress is primarily distributed at the top and bottom of the model, and the minimum displacement is concentrated between the horizontal connections of the two circular holes, i.e., the distribution of the minimum displacement in the NM-3 model is at 45° between the two circular holes. At the peak stress, the small-displacement area is still concentrated between the two circular holes, whereas the displacement outside the two circular holes increases rapidly. For example, the displacement outside the two circular holes in the NM-3

model changes into a concentrated area of the maximum displacement. At this time, the displacement field distribution in the middle of the model is chaotic, indicating that large critical failure cracks occur in some areas, affecting the displacement field distribution. At the postpeak failure stage, NM-2 shows apparent fracture failure on both sides of the model (outside of the two holes) and in the middle of the circular hole. The NM-3 model is split near the two circular holes in the model's lower left and upper right areas. In the small-displacement area of the NM-4 model at the failure stage, the main circular holes below show a small "V" distribution with vertices, while the entire model reveals fracture failure at the outer and lower circular holes on both sides of the "V" distribution to the bottom of the model.

Before the peak stress, the displacement field variation pattern of the NM-5 to NM-7 models is similar to that of the corresponding two-hole models. The regions with small displacement are also mainly distributed between the holes. However, the displacement field distribution at the peak stress is more disorderly than that of the corresponding two-hole models due to the influence of the three circular holes. In the failure period, the NM-5 model undergoes fracture failure along the outer side of the middle hole and the
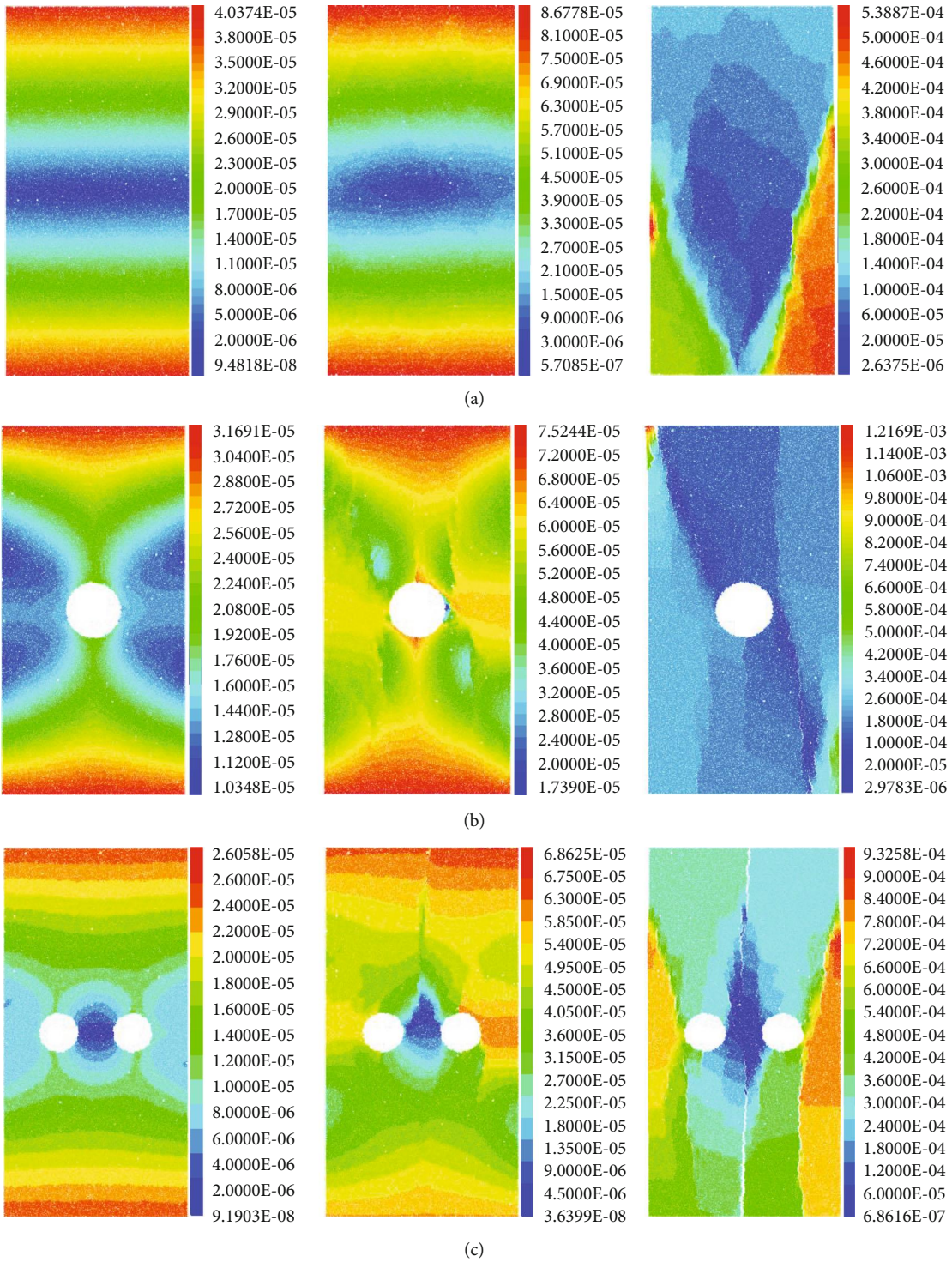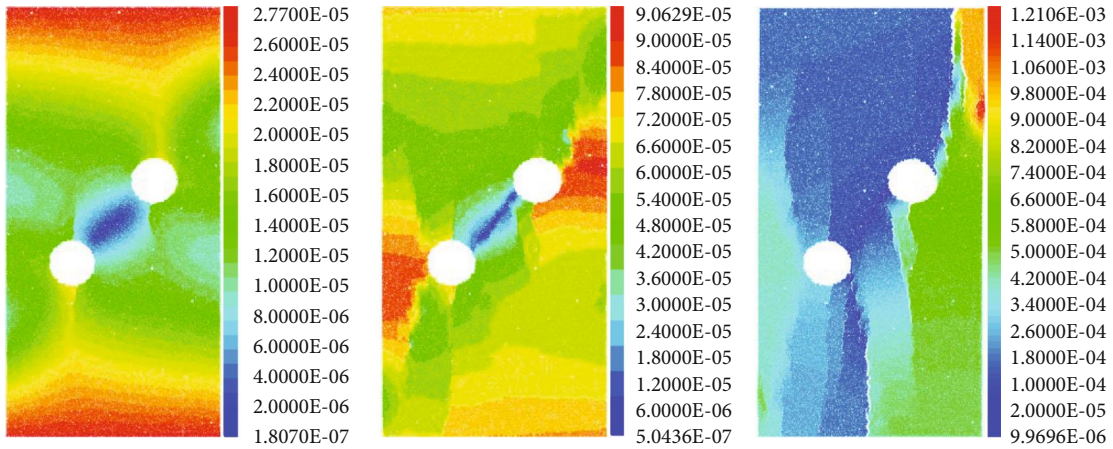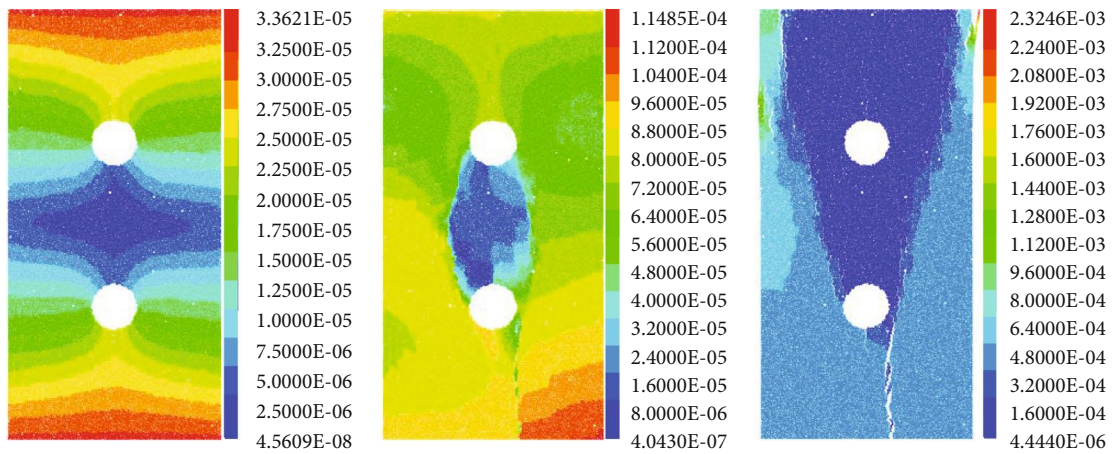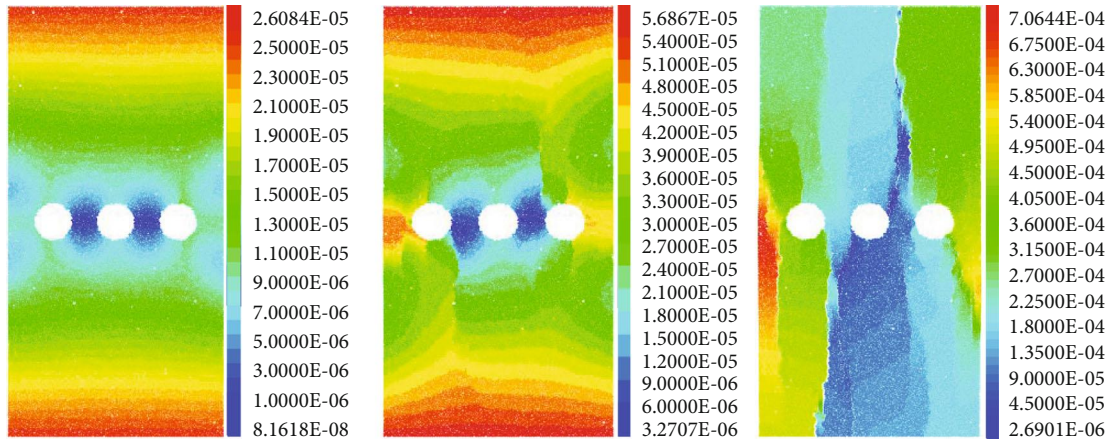
(a)

(b)

(c)

FIGURE 7: Continued.

(d)
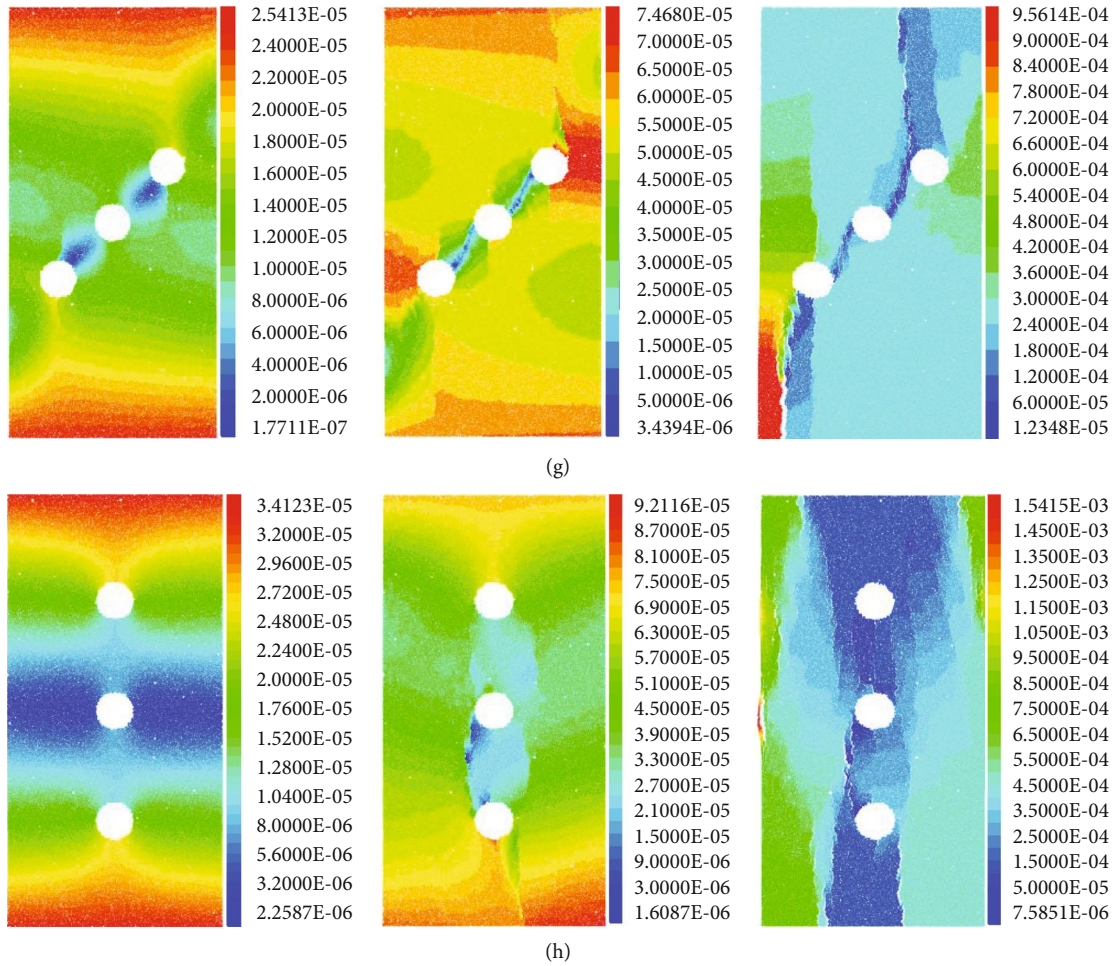

(e)

(f)

FIGURE 7: Continued.

(g)

(h)

Figure 7: Variations in the displacement fields: (a) represents the intact model; (b–h) represent the NM-1 model to the NM-7 model, respectively.

circular holes on both sides, and the maximum displacement area is distributed outside the circular holes on both sides of the model. In the NM-6 model, there is a fracture connection between the three circular holes, and splitting failure occurs along the upward and downward circular holes. The fracture failure of the NM-7 model mainly occurs on both sides of the three circular holes, demonstrating a relatively broken splitting failure. The analysis of the displacement field evolution shows that the distribution and number of circular holes play a vital role in the evolution of the displacement field and the failure mode of the models.

4. Discussion

This study used the PFC2D code to establish limestone models with different numbers and distributions of circular hole flaws under seven operating conditions. It considered the arrangement and number of holes as the main variables. If the number of holes increases, the distribution of holes will be involved. To better represent the effect of the number of holes on the damage and distinguishing failure features of the rock samples, the total flaw area in the model was kept

consistent, and the distance between holes and the model boundary was the same; most researchers did not consider these conditions. However, no specific analysis of other multihole models with different inclination arrangements, such as 30° or 60°, was performed to facilitate this study.

The models with various numbers and distributions of circular hole flaws in this research and the models in related studies [23–25, 27, 30, 31, 34] have some similar distribution arrangements. Although the aperture sizes of the circular holes set in previous models are frequently identical, the derived mechanical properties and deformation and failure behaviors of rocks with the same number and arrangement of hole defects are comparable to the results obtained, indicating the reliability of this study. Zhang et al. [59] also utilized the PFC2D code to investigate the changes in the mechanical parameters of the sandstone model with two circular holes arranged at various inclination angles and analyzed the damage variables of the models using the AE characteristics. However, the established models only contain two circular holes, large and small, without analyzing the evolution law of the entire process of the cracks and using the AE characteristics to determine the damage stress

of the models. Based on the difference in the number and distribution of holes, previous studies rarely addressed the effect of crack initiation stress and damage stress of defective rock samples. The study's results demonstrated that under the same number of circular holes, the crack initiation stress and damage stress of the model change with the distribution of holes in the shape of a "V", providing a valuable reference for analyzing the damage and failure of rock masses.

In addition, since the hole shape in this study was only circular, it cannot represent the complexity of natural rock masses with irregular defect shapes and uneven distribution of other defect shapes or types. However, based on the premise of the same flaw area, the variation of the mesomechanical behavior of a rock mass, such as the damage evolution caused by different numbers and distributions of circular hole flaws, was comprehensively analyzed. To a certain extent, this study provides insights into the interaction between the number and distribution of holes and their influence on the complex mechanical responses of rock masses.

5. Conclusions

(1) The number and distribution of circular hole defects greatly influence the peak stress, crack initiation stress, damage stress, and acoustic emission characteristics of rock samples. Due to the varying number and distribution of circular hole flaws, the peak stress, crack initiation, and damage stress of the single-hole model are between those of multihole models. For the models with two or three circular holes, the peak stress, damage stress, and crack initiation stress exhibit a "V"-shaped change as the angle of the hole arrangement rises, and the characteristic stress values are the highest when the hole flaws are arranged vertically

(2) The presence of hole flaws causes crack initiation at the top and bottom of the circular holes in the models, and the two models with circular holes arranged at 45° begin to crack earlier. In the process of each model reaching its peak stress, the crack development of the model with circular hole defects concentrates primarily near or between circular holes and extends outward from near or between circular holes until the entire model is essentially coalesced. Variations in the path, shape, and number of crack development are primarily due to differences in the number and distribution of circular holes

(3) Before the peak stress, stress concentration areas are formed near the circular holes in the models. With the different distribution of the circular hole defects, the stress release areas or the tensile stress areas remain concentrated at the upper and lower vertices of the circular hole, whereas the compressive stress concentration areas of the multihole arranged at 45° rotate with the connection area of the circular hole's center. The stress concentration

areas in the two models with vertical circular holes are still distributed on both sides of the models after their failure

(4) The number and distribution of the circular holes play a vital role in the evolution of the displacement field and the failure mode of the models. Before the peak stress, the small displacements of circular-holed models are concentrated near and between the circular holes and vary with the arrangement angle of the circular holes. In the failure stage, the fracture failure path of the entire model is affected by the different distributions of the circular holes, resulting in various failure patterns of the rock samples with distinct numbers and distributions of hole flaws

Data Availability

Some or all data, models, or code that support the findings of this study are available from the corresponding author upon reasonable request.

Conflicts of Interest

The authors declare no conflict of interest.

Acknowledgments

References

[1] R. L. Kranz, "Crack-crack and crack-pore interactions in stressed granite," *International Journal of Rock Mechanics and Mining Science and Geomechanics Abstracts*, vol. 16, no. 1, pp. 37–47, 1979.

[2] Z. L. Zhou, L. H. Tan, W. Z. Cao, Z. Y. Zhou, and X. Cai, "Fracture evolution and failure behaviour of marble specimens containing rectangular cavities under uniaxial loading," *Engineering Fracture Mechanics*, vol. 184, pp. 183–201, 2017.

[3] G. Q. Zhou, H. B. Yan, K. H. Chen, and R. T. Zhang, "Spatial analysis for susceptibility of second-time karst sinkholes: a case study of Jili village in Guangxi, China," *Computational Geosciences*, vol. 89, pp. 144–160, 2016.

[4] D. T. Nicholson, "Pore properties as indicators of breakdown mechanisms in experimentally weathered limestones," *Earth Surface Processes and Landforms*, vol. 26, no. 8, pp. 819–838, 2001.

[5] A. A. Al-Harthi, R. M. Al-Amri, and W. M. Shehata, "The porosity and engineering properties of vesicular basalt in Saudi Arabia," *Engineering Geology*, vol. 54, no. 3-4, pp. 313–320, 1999.

[6] L. W. Guo, S. L. Wang, L. M. Sun, Z. H. Kang, and C. J. Zhao, "Numerical simulation and experimental studies of karst caves collapse mechanism in fractured-vuggy reservoirs," *Geofluids*, vol. 2020, Article ID 8817104, 21 pages, 2020.

[7] A. Fakhimi, F. Carvalho, T. Ishida, and J. F. Labuz, "Simulation of failure around a circular opening in rock," *International Journal of Rock Mechanics and Mining Sciences*, vol. 39, no. 4, pp. 507–515, 2002.

[8] W. C. Zhu, J. Liu, C. A. Tang, X. D. Zhao, and B. H. Brady, "Simulation of progressive fracturing processes around underground excavations under biaxial compression," *Tunnelling and Underground Space Technology*, vol. 20, no. 3, pp. 231–247, 2005.

[9] H. Haeri, A. Khaloo, and M. F. Marji, "Fracture analyses of different pre-holed concrete specimens under compression," *Acta Mechanica Sinica*, vol. 31, no. 6, pp. 855–870, 2015.

[10] H. Y. Wang and Q. Zhang, "Mechanical behavior of frozen porous sandstone under uniaxial compression," *Geofluids, Article*, vol. 2021, article 1872065, 6 pages, 2021.

[11] Q. B. Lin, P. Cao, J. J. Meng, R. H. Cao, and Z. Y. Zhao, "Strength and failure characteristics of jointed rock mass with double circular holes under uniaxial compression: Insights from discrete element method modelling," *Theoretical and Applied Fracture Mechanics*, vol. 109, article 102692, 2020.

[12] X. R. Liu, S. Q. Yang, Y. H. Huang, and J. L. Cheng, "Experimental study on the strength and fracture mechanism of sandstone containing elliptical holes and fissures under uniaxial compression," *Engineering Fracture Mechanics*, vol. 205, pp. 205–217, 2019.

[13] S. Q. Yang, P. F. Yin, Y. C. Zhang et al., "Failure behavior and crack evolution mechanism of a non-persistent jointed rock mass containing a circular hole," *International Journal of Rock Mechanics and Mining Sciences*, vol. 114, pp. 101–121, 2019.

[14] W. Zeng, S. Q. Yang, and W. L. Tian, "Experimental and numerical investigation of brittle sandstone specimens containing different shapes of holes under uniaxial compression," *Engineering Fracture Mechanics*, vol. 200, pp. 430–450, 2018.

[15] Y. L. Gui, Z. Y. Zhao, C. Zhang, and S. Q. Ma, "Numerical investigation of the opening effect on the mechanical behaviours in rocks under uniaxial loading using hybrid continuum-discrete element method," *Computers and Geotechnics*, vol. 90, pp. 55–72, 2017.

[16] Z. G. Xia, S. J. Chen, X. Z. Liu, and R. Sun, "Strength characteristics and fracture evolution of rock with different shapes inclusions based on particle flow code," *Geomechanics and Engineering*, vol. 22, no. 5, pp. 461–473, 2020.

[17] D. Y. Li, Q. Q. Zhu, Z. L. Zhou, X. B. Li, and P. G. Ranjith, "Fracture analysis of marble specimens with a hole under uniaxial compression by digital image correlation," *Engineering Fracture Mechanics*, vol. 183, pp. 109–124, 2017.

[18] C. Zhao, H. Matsuda, C. Morita, and M. R. Shen, "Study on failure characteristic of rock-like materials with an open-hole under uniaxial compression," *Strain*, vol. 47, no. 5, pp. 405–413, 2011.

[19] C. G. Sammis and M. F. Ashby, "The failure of brittle porous solids under compressive stress states," *Acta Metallurgica*, vol. 34, no. 3, pp. 511–526, 1986.

[20] P. Lin, R. H. C. Wong, and C. A. Tang, "Experimental study of coalescence mechanisms and failure under uniaxial compression of granite containing multiple holes," *International Journal of Rock Mechanics and Mining Sciences*, vol. 77, pp. 313–327, 2015.

[21] S. Q. Yang, Y. H. Huang, W. L. Tian, and J. B. Zhu, "An experimental investigation on strength, deformation and crack evolution behavior of sandstone containing two oval flaws under uniaxial compression," *Engineering Geology*, vol. 217, pp. 35–48, 2017.

[22] W. L. Tian, S. Q. Yang, and Y. H. Huang, "Discrete element modeling on crack evolution behavior of sandstone containing two oval flaws under uniaxial compression," *Arabian Journal of Geosciences*, vol. 13, no. 11, p. 418, 2020.

[23] M. R. Du, H. W. Jing, H. J. Su, T. T. Zhu, and M. L. Chen, "Strength and failure characteristics of sandstone containing two circular holes filled with two types of inclusions under uniaxial compression," *Journal of Central South University*, vol. 24, no. 11, pp. 2487–2495, 2017.

[24] Z. L. Zhao, H. W. Jing, X. S. Shi, and G. S. Han, "Experimental and numerical study on mechanical and fracture behavior of rock-like specimens containing pre-existing holes flaws," *European Journal of Environmental and Civil Engineering*, vol. 26, no. 1, pp. 299–319, 2022.

[25] W. B. Ma, Y. L. Chen, W. Yi, and S. C. Guo, "Investigation on crack evolution behaviors and mechanism on rock-like specimen with two circular-holes under compression," *Theoretical and Applied Fracture Mechanics*, vol. 118, p. 103222, 2022.

[26] Z. C. He, F. Q. Gong, W. X. Wu, and W. H. Wang, "Experimental investigation of the mechanical behaviors and energy evolution characteristics of red sandstone specimens with holes under uniaxial compression," *Bulletin of Engineering Geology and the Environment*, vol. 80, no. 7, pp. 5845–5865, 2021.

[27] C. A. Tang, R. H. C. Wong, K. T. Chau, and P. Lin, "Modeling of compression-induced splitting failure in heterogeneous brittle porous solids," *Engineering Fracture Mechanics*, vol. 72, no. 4, pp. 597–615, 2005.

[28] H. D. Liu, S. Liu, Z. G. Xia, H. Guo, and Y. T. Yuan, "Study on mechanical properties and damage features of rock-coal-rock combination models with defects and fillings," *Geomechanics and Engineering*, vol. 27, no. 3, pp. 239–251, 2021.

[29] R. H. C. Wong, P. Lin, and C. A. Tang, "Experimental and numerical study on splitting failure of brittle solids containing single pore under uniaxial compression," *Mechanics of Materials*, vol. 38, no. 1-2, pp. 142–159, 2006.

[30] R. H. C. Wong and P. Lin, "Numerical study of stress distribution and crack coalescence mechanisms of a solid containing multiple holes," *International Journal of Rock Mechanics and Mining Sciences*, vol. 79, pp. 41–54, 2015.

[31] Y. L. Gui, J. L. Shang, J. J. Ma, and Z. Y. Zhao, "Numerical study of the circular opening effect on mechanical behaviour of rock under confinement," *Journal of Rock Mechanics and Geotechnical Engineering*, vol. 11, no. 6, pp. 1201–1210, 2019.

[32] Y. H. Huang, S. Q. Yang, P. G. Ranjith, and J. Zhao, "Strength failure behavior and crack evolution mechanism of granite containing pre-existing non-coplanar holes: experimental study and particle flow modeling," *Computers and Geotechnics*, vol. 88, pp. 182–198, 2017.

[33] C. Jespersen, M. Maclaughlin, and N. Hudyma, "Strength, deformation modulus and failure modes of cubic analog specimens representing macroporous rock," *International Journal of Rock Mechanics and Mining Sciences*, vol. 47, no. 8, pp. 1349–1356, 2010.

[34] Y. H. Huang, S. Q. Yang, and W. L. Tian, "Cracking process of a granite specimen that contains multiple pre-existing holes under uniaxial compression," *Fatigue and Fracture of Engineering Materials and Structures*, vol. 42, no. 6, pp. 1341–1356, 2019.

[35] S. Liu, H. D. Liu, H. N. Liu, Z. G. Xia, Y. W. Zhao, and J. Y. Zhai, "Numerical simulation of mesomechanical properties of limestone containing dissolved hole and persistent joint," *Theoretical and Applied Fracture Mechanics*, vol. 122, p. 103572, 2022.

[36] D. O. Potyondy and P. A. Cundall, "A bonded-particle model for rock," *International Journal of Rock Mechanics and Mining Sciences*, vol. 41, no. 8, pp. 1329–1364, 2004.

[37] S. J. Chen, Z. G. Xia, F. Feng, and D. W. Yin, "Numerical study on strength and failure characteristics of rock samples with different hole defects," *Bulletin of Engineering Geology and the Environment*, vol. 80, no. 2, pp. 1523–1540, 2021.

[38] Z. G. Xia, S. Liu, Z. Bian et al., "Mechanical properties and damage characteristics of coal-rock combination with different dip angles," *KSCE Journal of Civil Engineering*, vol. 25, no. 5, pp. 1687–1699, 2021.

[39] M. Bahaaddini, P. C. Hagan, R. Mitra, and B. K. Hebblewhite, "Scale effect on the shear behaviour of rock joints based on a numerical study," *Engineering Geology*, vol. 181, pp. 212–223, 2014.

[40] C. E. Fairhurst and J. A. Hudson, "Discussion," *International Journal of Rock Mechanics and Mining Science and Geomechanics Abstracts*, vol. 36, no. 3, pp. 279–289, 1999.

[41] U. Castro-Filgueira, L. R. Alejano, J. Arzúa, and D. M. Ivars, "Sensitivity analysis of the micro-parameters used in a PFC analysis towards the mechanical properties of rocks," *Process Engineering*, vol. 191, pp. 488–495, 2017.

[42] A. Lisjak and G. Grasselli, "A review of discrete modeling techniques for fracturing processes in discontinuous rock masses," *Journal of Rock Mechanics and Geotechnical Engineering*, vol. 6, no. 4, pp. 301–314, 2014.

[43] H. D. Liu, S. Liu, Y. W. Zhao et al., "Numerical simulation of the effect of internal hole defect size on the mechanical properties of limestone," *PLoS One*, vol. 17, no. 10, 2022.

[44] J. W. Fu, H. Haeri, M. D. Yavari, V. Sarfarazi, and M. F. Marji, "Effects of the measured noise on the failure mechanism of pre-cracked concrete specimens under the loading modes I, II, III, and IV," *Strength of Materials*, vol. 53, no. 6, pp. 938–949, 2021.

[45] J. W. Fu, M. D. Guo, H. Haeri, V. Sarfarazi, and M. F. Marji, "A discrete element analysis of the indirect tensile failure in hollow Brazilian discs of bedded geo-materials," *Strength of Materials*, vol. 54, no. 3, pp. 462–472, 2022.

[46] V. Sarfarazi, H. Haeri, A. B. Shemirani, and Z. Zhu, "Shear behavior of non-persistent joint under high normal load," *Strength of Materials*, vol. 49, no. 2, pp. 320–334, 2017.

[47] J. F. Hazzard, R. P. Young, and S. C. Maxwell, "Micromechanical modeling of cracking and failure in brittle rocks," *Journal of Geophysical Research*, vol. 105, no. B7, pp. 16683–16697, 2000.

[48] J. W. Fu, H. Haeri, V. Sarfarazi, A. H. Noshadi, M. F. Marji, and M. D. Guo, "Investigating the failure behavior of gypsum specimens with non-persistent vertical notch under uniaxial compression," *Strength of Materials*, vol. 54, no. 1, pp. 14–32, 2022.

[49] H. Haeri, V. Sarfarazi, and Z. Zhu, "Effect of normal load on the crack propagation from pre-existing joints using particle flow code (PFC)," *Computers and Concrete*, vol. 19, no. 1, pp. 99–110, 2017.

[50] Z. J. Wen, X. Wang, L. J. Chen, G. Lin, and H. L. Zhang, "Size effect on acoustic emission characteristics of coal-rock damage evolution," *Advances in Materials Science and Engineering*, vol. 2017, Article ID 3472485, 8 pages, 2017.

[51] Q. Ma, Y. L. Tan, X. S. Liu, Q. H. Gu, and X. B. Li, "Effect of coal thicknesses on energy evolution characteristics of roof rock- coal-floor rock sandwich composite structure and its damage constitutive model," *Composites Part B: Engineering*, vol. 198, article 108086, 2020.

[52] J. Lemaitre, J. P. Sermage, and R. Desmorat, "A two scale damage concept applied to fatigue," *International Journal of Fracture*, vol. 97, pp. 67–81, 1999.

[53] E. Eberhardt, D. Stead, B. Stimpson, and R. S. Read, "Identifying crack initiation and propagation thresholds in brittle rock," *Canadian Geotechnical Journal*, vol. 35, no. 2, pp. 222–233, 1998.

[54] C. D. Martin and N. A. Chandler, "The progressive fracture of Lac du Bonnet granite," *International Journal of Rock Mechanics and Mining Science and Geomechanics Abstracts*, vol. 31, no. 6, pp. 643–659, 1994.

[55] F. Pelli, P. K. Kaiser, and N. R. Morgenstern, "An interpretation of ground movements recorded during construction of the Donkin-Morien tunnel," *Canadian Geotechnical Journal*, vol. 28, no. 2, pp. 239–254, 1991.

[56] J. Kim, J. Yi, J. Kim, G. Zi, and J. S. Kong, "Fatigue life prediction methodology using entropy index of stress interaction and crack severity index of effective stress," *International Journal of Damage Mechanics*, vol. 22, no. 3, pp. 375–392, 2013.

[57] M. Prudencio and M. V. S. Jan, "Strength and failure modes of rock mass models with non-persistent joints," *International Journal of Rock Mechanics and Mining Sciences*, vol. 44, no. 6, pp. 890–902, 2007.

[58] H. Mokhtarian, H. Moomivand, and H. Moomivand, "Effect of infill material of discontinuities on the failure criterion of rock under triaxial compressive stresses," *Theoretical and Applied Fracture Mechanics*, vol. 108, p. 102652, 2020.

[59] Q. Zhang, X. Wang, L. G. Tian, and D. M. Huang, "Analysis of mechanical and acoustic emission characteristics of rock materials with double-hole defects based on particle flow code," *Shock and Vibration*, vol. 2018, Article ID 7065029, 11 pages, 2018.